

# Tensor Tilt from Primordial B-modes

Brian A. Powell<sup>\*</sup>

*Institute for Defense Analyses, Alexandria, Virginia, 22311*

7 October 2011

## ABSTRACT

A primordial cosmic microwave background B-mode is widely considered a “smoking gun” signature of an early period of inflationary expansion. However, competing theories of the origin of structure, including string gases and bouncing cosmologies, also produce primordial tensor perturbations that give rise to a B-mode. These models can be differentiated by the scale dependence of their tensor spectra: inflation predicts a red tilt ( $n_T < 0$ ), string gases and loop quantum cosmology predict a blue tilt ( $n_T > 0$ ), while a nonsingular matter bounce gives zero tilt ( $n_T = 0$ ). We perform a Bayesian analysis to determine how far  $|n_T|$  must deviate from zero before a tilt can be detected with current and future B-mode experiments. We find that Planck in conjunction with QUIET (II) will decisively detect  $n_T \neq 0$  if  $|n_T| > 0.3$ , too large to distinguish either single field inflation or string gases from the case  $n_T = 0$ . While a future mission like CMBPol will offer improvement, only an ideal satellite mission will be capable of providing sufficient Bayesian evidence to distinguish between each model considered.

**Key words:** early Universe – inflation – cosmic background radiation – methods: statistical.

## 1 INTRODUCTION

Precision cosmology is on the verge of answering deep questions about the early Universe. Are the temperature fluctuations of the cosmic microwave background (CMB) Gaussian? Will we discover primordial tensor modes in the CMB? The existence of a large-scale spectrum of tensor perturbations is widely considered to be indicative of an early period of inflation – a “smoking gun” signature of quasi-de Sitter expansion; however, inflation is not the only source (Brandenberger 2011). Alternative theories of the origin of structure, like string gas cosmology or bouncing Universe models, are capable of generating B-modes, as are topological defects (Seljak & Slosar 2006; Pogosian & Wyman 2008) and bubble collisions from phase transitions (Jones-Smith et al. 2008) occurring after the big bang. These latter two sources have the potential to obscure or confuse the signal from inflation or its alternatives, but future observations should be able to disentangle the sources if the primordial signal is large enough (Urrestilla et al. 2008; Baumann & Zaldarriaga 2009; Garcia-Bellido et al. 2011). The purpose of the present paper is to investigate how well the different *primordial* sources of tensor modes – inflation, string gases, or bounces – can be resolved and supported.

The tensor perturbation spectrum is typically modeled as a power law in comoving wavenumber,  $k$ ,

$$P_h(k) = P_h(k_0) \left( \frac{k}{k_0} \right)^{n_T}, \quad (1)$$

where  $n_T$  is the tensor spectral index. In slow roll inflation the amplitude of tensors is determined by the Hubble parameter,  $P_h \propto H^2$ , which, together with  $\dot{H} < 0$  in the Friedmann Universe, furnishes the hallmark prediction of a red spectrum:  $n_T < 0$ . Meanwhile, the spectrum of metric fluctuations that arises from a string gas in the early Universe is characterized by  $n_T > 0$  in the string frame (Brandenberger et al. 2007), due to the growth of anisotropic stress as the radiation dominated phase is approached. A blue spectrum can also be generated during a phase of so-called superinflation (Piao & Zhang 2004), motivated, for example, by loop quantum cosmology (Bojowald 2002). Yet a different picture emerges from fluctuations produced during the contracting phase of a bouncing cosmology: a matter dominated contraction with a regular bounce gives a scale invariant spectrum in the expanding radiation dominated phase (Wands 1999; Finelli & Brandenberger 2008). Evidently, the *sign* of  $n_T$  is a more likely indicator of inflation than the mere presence of tensors. But how large must this tilt be in order for current and future probes to detect it with confidence?

The basic question that we seek to answer in this work

<sup>\*</sup> E-mail: brian.powell007@gmail.com

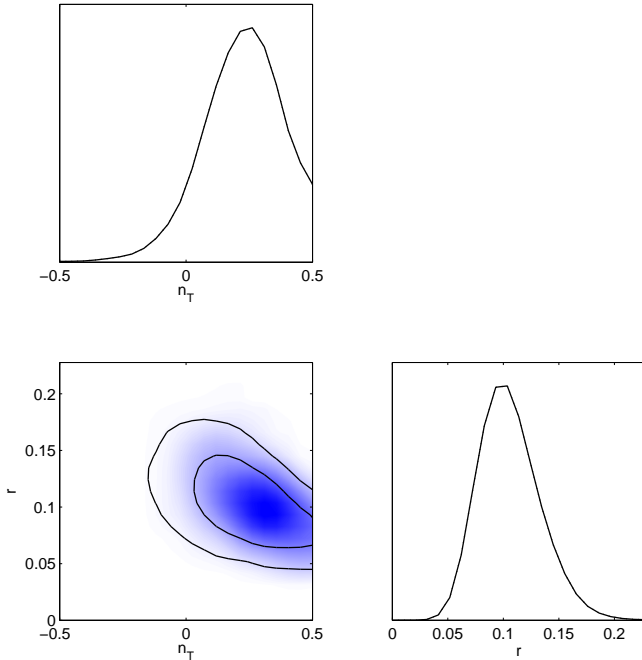


**Figure 1.** A simulated  $2\sigma$  detection of  $n_T \neq 0$  obtained from mock Planck data with a fiducial tensor spectrum  $r = 0.1$  and  $n_T = 0.3$ .

is how far  $n_T$  must deviate from zero before one can confidently conclude  $n_T \neq 0$ . From the point of view of sampling statistics, this is a straightforward hypothesis test: how large must  $n_T$  be in order to reject the null hypothesis,  $\mathcal{H}_0 : n_T = 0$ ? Having analyzed data,  $d$ , one determines whether the best fit value,  $\bar{n}_T$ , is a sufficient number of standard deviations,  $\sigma_{n_T|d}$ , away from  $n_T = 0$  to satisfy the chosen significance level,  $\alpha$ . Specifically, assuming that  $n_T$  is Gaussian distributed, the p-value must be calculated,

$$p = \frac{1}{\sqrt{2\pi}} \int_s^\infty e^{-z^2/2} dz \leq \frac{\alpha}{2}, \quad (2)$$

where the test statistic  $s = |\bar{n}_T|/\sigma_{n_T|d}$  is the number of standard deviations that  $\bar{n}_T$  lies away from  $n_T = 0$ . For example, the significance level  $\alpha = 0.05$  corresponds to  $s = 1.96$ , with the conclusion that one risks a 5% chance of falsely rejecting the null hypothesis,  $n_T = 0$ .

If one were to proceed along these lines, it would be determined that the Planck Surveyor<sup>1</sup> will detect  $n_T \neq 0$  at the 95% confidence level if  $|n_T| \geq 0.3$  for a tensor/scalar ratio  $r = 0.1$  (see Fig. 1.)<sup>2</sup> What this approach fails to determine, however, is whether there is a *need* for allowing  $n_T$  to vary in the first place: is the fit to the data sufficiently improved to warrant the inclusion of  $n_T$  as a free parameter? The accepted approach to this problem is to apply Bayesian inference to the space of competing models. As a definition of *model*, we should have in mind a collec-

tion of parameters,  $\theta = (\theta_1, \dots, \theta_n)$ , with associated prior probabilities  $\pi(\theta_1), \dots, \pi(\theta_n)$ . Here we have two models:  $\mathcal{H}_0$  corresponds to the null hypothesis in which  $n_T = 0$ , and  $\mathcal{H}_1$  contains  $n_T$  as a parameter free to vary across some prior range,  $[n_{T,\min}, n_{T,\max}]$ .

Bayesian analysis gives preference to the least complex model that best fits the data (MacKay 2003; Trotta 2005; Liddle et al. 2006; Mukherjee & Parkinson 2010; Trotta 2008). Models with many parameters free to vary across large prior ranges,  $\Delta\theta_j \sim 1/\pi(\theta_j)$ , are considered more complex than models with fewer parameters and more restrictive priors. Bayesian selection prefers models that are *predictive*: the prior and posterior parameter widths should be comparable. Frequentist significance tests like Eq. (2) do not incorporate this essential aspect of model selection, and can sometimes give conclusions in striking disagreement with Bayesian inference (Lindley 1957; Shafer 1982; Trotta 2005). This disagreement, known as Lindley's paradox, tends to be most prevalent for detections in the range of two to four  $\sigma$  (Trotta 2005): the same threshold at which the sampling statistics hypothesis test Eq. (2) will detect  $n_T = 0.3$  with Planck. In this work, we do not solely examine how well future probes might constrain  $n_T$ , an analysis carried out in detail by others (Verde et al. 2006; Zhao & Zhang 2009; Ma et al. 2010); we are instead interested in going one step further, and determining whether or not, given these constraints, we are warranted in including  $n_T$  as a free parameter. In the next section, we develop the framework for performing Bayesian model comparison forecasts for future experiments, following closely the approach taken by (Pahud et al. 2006) and (Vardanyan et al. 2006) to investigate the tilt of the scalar spectrum and the curvature of the Universe, respectively.

## 2 BAYESIAN EVIDENCE

Methods of Bayesian inference can be applied to the problem of model selection in a manner fully consistent with probability theory. Given a model,  $\mathcal{H}_i$ , and a dataset,  $\mathbf{d}$ , Bayes' Theorem gives

$$p(\mathcal{H}_i|\mathbf{d}) = \frac{p(\mathbf{d}|\mathcal{H}_i)\pi(\mathcal{H}_i)}{\pi(\mathbf{d})}, \quad (3)$$

where the quantity  $p(\mathcal{H}_i|\mathbf{d})$  is the posterior probability of the model  $\mathcal{H}_i$ , and  $p(\mathbf{d}|\mathcal{H}_i)$  is the *evidence* for model  $\mathcal{H}_i$ . One typically assigns equal prior probabilities  $\pi(\mathcal{H}_i)$  to the alternative models, and  $\pi(\mathbf{d})$  is independent of the model. If we again apply Bayes' theorem,

$$p(\theta|\mathbf{d}, \mathcal{H}_i) = \frac{p(\mathbf{d}|\theta, \mathcal{H}_i)\pi(\theta|\mathcal{H}_i)}{p(\mathbf{d}|\mathcal{H}_i)}, \quad (4)$$

we obtain the posterior probability of the parameters  $\theta$  given  $\mathbf{d}$ . The term  $p(\mathbf{d}|\theta, \mathcal{H}_i)$  is a function of both the parameter values and the data; for a given dataset, it is commonly called the likelihood of the parameters,  $\mathcal{L}(\theta|\mathbf{d}, \mathcal{H}_i)$ . The evidence from Eq. (3) is nothing more than a normalization constant for Eq. (4),

$$p(\mathbf{d}|\mathcal{H}_i) = \int \mathcal{L}(\theta|\mathbf{d}, \mathcal{H}_i)\pi(\theta|\mathcal{H}_i)d\theta. \quad (5)$$

This expression defines the evidence to be the prior-weighted average of the likelihood over the parameter space.

<sup>1</sup> <http://www.esa.int/planck>

<sup>2</sup> This result is obtained without the assumption of Gaussianity leading to Eq. (2), but instead follows from a Bayesian parameter estimation performed on a simulated Planck-precision data set with fiducial tensor spectrum  $r = 0.1$  and  $n_T = 0.3$ . We will discuss our analytical method in detail in the following sections.

For the sake of illustration, assume that the parameter  $\theta_j$  is well constrained by some data,  $\mathbf{d}$ , so that the posterior probability  $p(\theta_j|\mathbf{d}, \mathcal{H}_i)$  is well-peaked within the prior range,

$$\pi(\theta_j|\mathcal{H}_i) = [H(\theta_j - \theta_{j,\min})H(\theta_{j,\max} - \theta_j)] \frac{1}{\Delta\theta_j}, \quad (6)$$

where  $H$  is a step function that enforces the prior range and we have chosen a *flat* prior on  $\theta_j$ ,  $\pi(\theta_j) = 1/\Delta\theta_j$ , within this range. Since the posterior distribution is well-peaked, we can approximate the integral Eq. (5) using Laplace's method with Eq. (4): we simply multiply the height of the unnormalized posterior (the numerator in Eq. (4)),  $\tilde{p}(\bar{\theta}_j|\mathbf{d}, \mathcal{H}_i)$ , by its width,  $\sigma_{\theta_j|d}$ ,

$$\begin{aligned} p(\mathbf{d}|\mathcal{H}_i) &= \int \tilde{p}(\theta_j|\mathbf{d}, \mathcal{H}_i) d\theta_j, \\ &\simeq \tilde{p}(\bar{\theta}_j|\mathbf{d}, \mathcal{H}_i) \times \sigma_{\theta_j|d}, \end{aligned} \quad (7)$$

where  $\bar{\theta}_j$  denotes the point of maximum likelihood. In terms of the likelihood function this becomes,

$$\begin{aligned} p(\mathbf{d}|\mathcal{H}_i) &\simeq \mathcal{L}(\bar{\theta}_j|\mathbf{d}, \mathcal{H}_i) \pi(\theta_j|\mathcal{H}_i) \sigma_{\theta_j|d}, \\ &\simeq \mathcal{L}(\bar{\theta}_j|\mathbf{d}, \mathcal{H}_i) \frac{\sigma_{\theta_j|d}}{\Delta\theta_j}. \end{aligned} \quad (8)$$

While only an approximation, this expression nicely reveals the essential ingredients of Bayesian model selection: a high-valued maximum likelihood clearly increases the evidence in favor of the model, while the *Occam factor*,  $\beta = \sigma_{\theta_j|d}/\Delta\theta_j \leq 1$ , penalizes overly complex or poorly predictive models. Models with a prior volume much larger than the posterior volume,  $\beta \ll 1$ , are not considered predictive because they can accommodate a wide range of parameter values before the data is collected. Complex models with loose priors and many free parameters that are well-constrained by the data are therefore penalized by the Occam factor, and will consequently have lower evidence than a simpler, more predictive model that fits the data equally well.

We are now ready to do model selection: we simply compute the Bayesian evidence for each model and compare. Given two competing models,  $\mathcal{H}_0$  and  $\mathcal{H}_1$ , this can be done via the Bayes factor,

$$B_{01} = \frac{p(\mathbf{d}|\mathcal{H}_0)}{p(\mathbf{d}|\mathcal{H}_1)}. \quad (9)$$

A rubric for scoring the significance of a model is given by the well-known Jeffreys' scale (Jeffreys 1961). The scale rates:  $|\ln B_{01}| < 1$  (indecisive),  $1 < |\ln B_{01}| < 2.5$  (substantial),  $2.5 < |\ln B_{01}| < 5$  (strong), and  $|\ln B_{01}| > 5$  (decisive), with  $\ln B_{01} > 0$  ( $\ln B_{01} < 0$ ) favoring  $\mathcal{H}_0$  ( $\mathcal{H}_1$ ). In this work, we will quote results for strong and decisive evidence, corresponding to odds ratios of 12:1 and 150:1, respectively.

While the Laplace method is instructive, it is not sufficient for an accurate determination of the evidence. While evaluating the integral in Eq. (5) is computationally demanding, various methods have been applied to problems of model selection in astrophysics, including nested sampling (Skilling 2004; Mukherjee et al. 2006) and thermodynamic integration (O'Ruanidh et al. 1996; Beltran et al. 2005). Here we make use of the *Savage-Dickey density ratio* (Dickey 1971), an exact analytical expression for  $B_{01}$  that can be applied whenever the models to be compared are nested. Models  $\mathcal{H}_0$  and  $\mathcal{H}_1$  share the same cosmological parameters,  $\psi$ , except for  $n_T$  which is set to zero in  $\mathcal{H}_0$ . For

separable priors,  $\pi(\psi|n_T, \mathcal{H}_1)|_{n_T=0} = \pi(\psi|\mathcal{H}_0)$ , the Bayes factor takes the form

$$B_{01} = \frac{p(n_T|\mathbf{d}, \mathcal{H}_1)}{\pi(n_T|\mathcal{H}_1)} \Big|_{n_T=0}, \quad (10)$$

where  $p(n_T|\mathbf{d}, \mathcal{H}_1)|_{n_T=0}$  is the marginalized posterior probability of  $n_T$  under model  $\mathcal{H}_1$ ,

$$p(n_T|\mathbf{d}, \mathcal{H}_1) = \int \mathcal{L}(\{\psi, n_T\}|\mathbf{d}, \mathcal{H}_1) d\psi, \quad (11)$$

evaluated at  $n_T = 0$ . This quantity can be obtained relatively easily using Markov Chain Monte Carlo (MCMC) techniques, and, in principle, gives  $B_{01}$  as a function of  $n_T$ . This is the function that we seek to determine in this analysis, for a variety of current and proposed CMB experiments. For each experiment, we will obtain projections by generating simulated CMB data across a range of values of  $n_T$ , and determine how the evidence for  $\mathcal{H}_1$  builds as  $|n_T|$  grows.

### 3 CMB SPECTRA FROM FUTURE PROBES

Primordial perturbations impart inhomogeneities in the photon temperature at decoupling, measured today as directional anisotropies on the last scattering sphere,

$$\frac{\delta T(\mathbf{n})}{T} = \sum_{\ell, m} a_{\ell m}^T Y_{\ell m}(\mathbf{n}), \quad (12)$$

where the multipole moments,  $a_{\ell m}$ , are complex Gaussian random variables with variance  $\langle a_{\ell m}^{T*} a_{\ell' m'}^T \rangle = C_\ell^{TT} \delta_{\ell\ell'} \delta_{mm'}$  in the direction  $\mathbf{n}$ . Quadrupolar temperature anisotropies at decoupling (and again at reionization) are projected into anisotropies in the polarization of the CMB and can be similarly decomposed (Kamionkowski et al. 1997),

$$\frac{\mathcal{P}_{ab}}{T} = \sum_{\ell m} \left[ a_{\ell m}^E Y_{(\ell m)ab}^E(\mathbf{n}) + a_{\ell m}^B Y_{(\ell m)ab}^B(\mathbf{n}) \right], \quad (13)$$

where the  $Y_{(\ell m)ab}^{E,B}$  are electric-type (curl-free) and magnetic-type (divergence-free) tensor spherical harmonics, respectively. The polarization anisotropies are described by the correlations,

$$\langle |a_{\ell m}^E|^2 \rangle = C_\ell^{EE}, \quad \langle |a_{\ell m}^B|^2 \rangle = C_\ell^{BB}, \quad (14)$$

and one nonzero cross correlation,

$$\langle a_{\ell m}^{T*} a_{\ell m}^E \rangle = C_\ell^{TE}. \quad (15)$$

Primordial density perturbations can be constrained by measurements of the temperature and E-mode polarization anisotropies, while primordial gravitational waves additionally create a B-mode polarization pattern (Kamionkowski et al. 1997; Seljak & Zaldarriaga 1997). The B-mode signal is therefore a key indicator of primordial tensors.

Our projections are based on simulated datasets. Since we do not have access to the true distribution of the  $a_{\ell m}$ 's, an estimator is formed from their measured values,

$$\hat{C}_\ell^{XY} = \sum_{m=-\ell}^{\ell} \frac{|a_{\ell m}^{X*} a_{\ell m}^Y|}{2\ell + 1}, \quad (16)$$

where  $XY = TT, EE, BB$ , and  $TE$ . As the sum of the squares of Gaussian random variables, the  $\hat{C}_\ell^{XY}$  are  $\chi^2_\nu$ -distributed with  $\nu = 2\ell + 1$  degrees of freedom. We generate simulated data by drawing the  $\hat{C}_\ell^{XY}$ 's from a  $\chi^2_{2\ell+1}$  distribution with variances (Knox 1995),

$$(\Delta\hat{C}_\ell^{XX})^2 = \frac{2}{(2\ell+1)f_{\text{sky}}} \left( C_\ell^{XX} + N_\ell^{XX} \right), \quad (17)$$

$$(\Delta\hat{C}_\ell^{TE})^2 = \frac{2}{(2\ell+1)f_{\text{sky}}} \left[ \left( C_\ell^{TE} \right)^2 + \left( C_\ell^{TT} + N_\ell^{TT} \right) \times \left( C_\ell^{EE} + N_\ell^{EE} \right) \right], \quad (18)$$

where  $f_{\text{sky}}$  is the fraction of sky covered, the  $C_\ell^{XY}$  are the theoretical signal spectra, and the  $N_\ell^{XY}$  are instrumental noise spectra for  $X = T, E$ , and  $B$ . For experiments with multiple frequency channels,  $c$ , the full noise spectrum is the inverse sum of the individual spectra over the channels,

$$N_\ell^{XY} = \left( \sum_c N_{\ell,c}^{XY} \right)^{-1}. \quad (19)$$

Assuming a Gaussian beam, the noise spectrum characterizes the combined effects of the instrument beam smearing and Gaussian white pixel noise,

$$N_\ell^{XY} = (\sigma_{\text{pix}}^X \theta_{\text{fwhm}})^2 \exp \left[ \ell(\ell+1) \frac{\theta_{\text{fwhm}}^2}{8 \ln 2} \right] \delta_{XY}, \quad (20)$$

where  $\sigma_{\text{pix}}^X$  is the noise per pixel (with  $\sigma_{\text{pix}}^P = \sqrt{2}\sigma_{\text{pix}}^T$ ),  $\theta_{\text{fwhm}}$  is the full width at half maximum (FWHM) of the Gaussian beam, and pixel noise from temperature and polarization maps is uncorrelated and taken to vanish.

We obtain projections for the Planck Surveyor, both alone and in combination with the ground-based telescopes PolarBear<sup>3</sup> and the Q/U Imaging Experiment (QUIET)<sup>4</sup>, the proposed CMBPol satellite mission (Baumann et al. 2009), and an ideal satellite. The satellite missions are sensitive to both the temperature and polarization spectra, while the ground-based experiments will measure only polarization. The two platforms are also sensitive to B-modes in different ranges: satellites are most sensitive to the reionization hump at  $\ell < 10$ , while ground-based detectors will perform best at intermediate scales,  $\ell = 30 - 500$ , probing the anisotropy at decoupling. In Figure 2 we show the S/N ratios of the experiments considered in this analysis as a function of multipole number,  $\ell$ , for a B-mode signal with  $r = 0.1$ .

For Planck, we include three channels with frequencies (100 GHz, 143 GHz, 217 GHz) and noise levels per beam  $(\sigma_{\text{pix}}^T)^2 = (46.25 \mu\text{K}^2, 36 \mu\text{K}^2, 17.6 \mu\text{K}^2)$ . The FWHM of the three channels are  $\theta_{\text{fwhm}} = (9.5', 7.1', 5.0')$  (Planck 2006). For PolarBear we consider frequency channels (90 GHz, 150 GHz, 220 GHz) with  $(\sigma_{\text{pix}}^T)^2 = (2.6 \mu\text{K}^2, 5.8 \mu\text{K}^2, 744 \mu\text{K}^2)$  and resolutions  $\theta_{\text{fwhm}} = (6.7', 4.0', 2.7')$ , and for QUIET (II) we use frequencies (60 GHz, 90 GHz) with  $(\sigma_{\text{pix}}^T)^2 = (0.04 \mu\text{K}^2, 0.08 \mu\text{K}^2)$  and  $\theta_{\text{fwhm}} = (23', 10')$  (Samtleben et al. 2007). We assume integration times of 0.5 and 3 years for these two experiments, respectively. We combine three channels for CMBPol with frequencies (100 GHz,

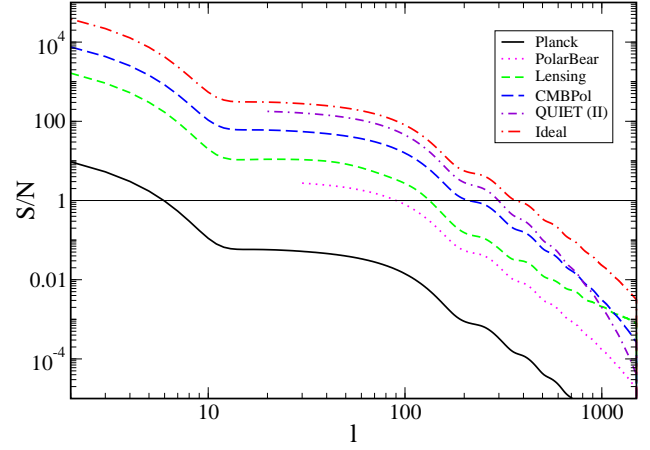


**Figure 2.** Signal-to-noise ratios of experiments considered in this analysis as a function of multipole number,  $\ell$ , based on a fiducial model with  $r = 0.1$ .

150 GHz, 220 GHz) and noise levels  $(\sigma_{\text{pix}}^T)^2 = (729 \text{ nK}^2, 676 \text{ nK}^2, 1600 \text{ nK}^2)$  and  $\theta_{\text{fwhm}} = (8', 5', 3.5')$  (Fraisie et al. 2008). In Figure 2, for reference, we also include the S/N ratio with lensing as the only noise source (green dashed). This contamination, arising from the gravitational lensing by large scale structure of primordial E-modes into B-modes (Zaldarriaga & Seljak 1998), dominates the signal at  $\ell > 100$ ; probes that seek to measure the B-mode signal in this range must successfully subtract the lensing contribution. This effect helps motivate our selection of experiments: PolarBear's sensitivity lies just below the lensing signal, while the full capability of the upgraded QUIET (II) and CMBPol will be more sensitive and require successful delensing (Hu & Okamoto 2002; Hirata & Seljak 2003). We assume for these experiments that lensing is reduced to a level of  $5 \times 10^{-8} \mu\text{K}^2$  (Seljak & Hirata 2004). Lastly, our ideal experiment will suffer from zero instrumental noise or beam effects, but will still be limited by cosmic variance,  $(\Delta\hat{C}_\ell)^2 = 2C_\ell^2/(2\ell+1)$ , and the reduced lensing noise. We assume sky coverages of  $f_{\text{sky}} = 0.65, 0.012, 0.04, 0.8$ , and  $1.0$ , respectively, for the experiments just listed. We next present our analysis and results.

## 4 EVIDENCE FOR A TENSOR TILT

The determination of how  $B_{01}$  varies with  $n_T$  requires an evaluation of  $p(n_T|\mathbf{d}, \mathcal{H}_1)$  (c.f. Eq. 9) across a range of  $n_T$ , although, in general, this distribution also depends implicitly on  $r$  ( $\sigma_{n_T}$  is an increasing function of  $r$ .) We first confront the simpler task of obtaining results for  $B_{01}$  with the fiducial tensor amplitude fixed at  $r = 0.1$ , near the upper 95% C.L. set by WMAP+BAO+ $H_0$  (Komatsu et al. 2011). Though limited, this provides an optimistic projection and filters out those experiments that fail to provide strong evidence for  $n_T \neq 0$  even under the most favorable conditions; those experiments that do provide strong evidence are analyzed further for the case of variable  $r$ .

<sup>3</sup> <http://bolo.berkeley.edu/polarbear>

<sup>4</sup> <http://quiet.uchicago.edu>

#### 4.1 Optimistic Projection

For each experiment listed in the previous section, we obtain  $p(n_T|\mathbf{d}, \mathcal{H}_1)$  by analyzing simulated data generated from the model  $\mathcal{H}_1$ . We assign the base cosmological parameters the fiducial values  $\Omega_b h^2 = 0.022$ ,  $\Omega_c h^2 = 0.105$ ,  $\theta_s = 1.04$ ,  $\tau = 0.09$ ,  $A_s = 2.23 \times 10^{-9}$ ,  $n_s = 0.97$ ,  $r = 0.1$ , and simulate a different dataset as  $n_T$  is incremented in steps of  $|\delta_{n_T}| = 0.1$  across the prior range  $n_T \in [-0.5, 0.5]^5$ . We use MCMC to constrain  $r$  and  $n_T$  for each dataset; since the base parameters  $\Omega_b h^2$ ,  $\Omega_c h^2$ ,  $\theta_s$ ,  $\tau$ ,  $A_s$ , and  $n_s$  have little effect on the B-mode signal, we only vary  $r$  and  $n_T$  within the chains. The theoretical temperature and polarization  $C_\ell$ -spectra are generated out to  $\ell = 2000$  with CAMB<sup>6</sup> (Lewis et al. 2000), and the parameter estimation is performed using CosmoMC<sup>7</sup> (Lewis & Bridle 2002). For each dataset, convergence is measured across four chains using the Gelman-Rubin R statistic. The constraints on  $r$  and  $n_T$  are in general correlated, but the parameter uncertainties can be minimized by choosing the pivot scale corresponding to the multipole at which they become uncorrelated,  $k_* \simeq 10^{-4} \text{Mpc}^{-1} \ell_*$ . This pivot scale depends on the data, and will be different for each experiment:  $\ell_* = 10, 30, 65, 150$ , and 300 for Planck, Planck+PolarBear, Planck+QUIET (II), CMBPol, and the ideal experiment (Zhao & Baskaran 2009; Zhao & Zhang 2009). By constraining  $r(k_*)$ , we minimize the effects of correlations in our comparisons of constraints across experiments.

We present results in Figure 3 and Table 1. In Figure 3, the data points represent the actual evaluations of  $\ln B_{01}$ ; the curves are obtained via quadratic regression. The gray shaded region,  $n_T > 0.15$ , is ruled out by nucleosynthesis constraints on the energy density of gravitational waves with power law spectra (Stewart & Brandenberger 2008). We find that Planck by itself will not find decisive (strong) evidence for  $n_T \neq 0$  unless  $|n_T| > 0.5$  (0.43); in combination with PolarBear and QUIET (II), these same levels of evidence are achieved for  $|n_T| \approx 0.36$  (0.28) and 0.29 (0.25), respectively. These detection thresholds are ruled out for power law spectra. The constraint from nucleosynthesis should, however, be applied with care since the assumption of a power law tensor spectrum is not always appropriate<sup>8</sup>. Meanwhile, a future space-based mission with the specifications of CMBPol will provide decisive evidence of  $n_T \neq 0$  for  $|n_T| \geq 0.15$  – just on the edge of the excluded region, and strong evidence for  $|n_T| \geq 0.12$ . Lastly, an ideal satellite experiment will perform even better: not only will it support a decisive (strong) confirmation of  $n_T \neq 0$  for  $|n_T| > 0.03$  (0.025), but it will provide strong evidence for  $n_T = 0$ , *i.e.* favor the null hypothesis  $\mathcal{H}_0$ , if  $|n_T| < 0.01$ . These results are summarized in Table 1.

<sup>5</sup> The Bayes factor depends on the prior range, but only weakly: for example, doubling the range gives  $|\Delta \ln B_{01}| = \ln 2 = 0.7$ .

<sup>6</sup> <http://camb.info>

<sup>7</sup> <http://cosmologist.info/cosmomc>

<sup>8</sup> While power law tensor spectra are expected from slow roll inflation, the primordial gravitational waves generated in scenarios of loop quantum cosmology are strongly non-power law: while typically steeply blue ( $n_T \approx 2$ ) on CMB scales, they are scale invariant on smaller scales. We discuss this further in Section 5.

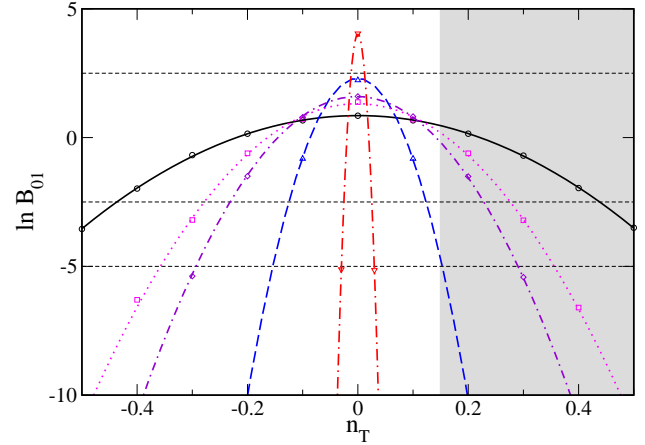


**Figure 3.** Bayes factor as a function of  $n_T$  with  $r = 0.1$  for the experiments discussed in the text: Planck (black solid), Planck+PolarBear (magenta dotted), Planck+QUIET (II) (purple dash dot), CMBPol (blue dashed), and ideal satellite (red long dash dot). The gray region is excluded for power laws by nucleosynthesis constraints.

**Table 1.** Fiducial  $n_T$  for which the different experiments will support strong ( $|\ln B_{01}| = 2.5$ ) and decisive ( $|\ln B_{01}| = 5$ ) evidence in favor of  $n_T \neq 0$  ( $\ln B_{01} < 0$ ) and  $n_T = 0$  ( $\ln B_{01} > 0$ ).

Experiment	$ n_T $ $\ln B_{01} = -2.5$	$ n_T $ $\ln B_{01} = -5$	$ n_T $ $\ln B_{01} = 2.5$
Planck	0.43	$> 0.5$	-
+PolarBear	0.28	0.36	-
+QUIET (II)	0.23	0.29	-
CMBPol	0.12	0.15	-
Ideal	0.025	0.03	0.01

#### 4.2 Dependence on $r$

The previous findings apply to  $\mathcal{H}_1$  with fiducial  $r = 0.1$ . However, the error on  $n_T$ , which largely determines the Bayes factor, depends on the base value of  $r$ . We now examine whether and how our conclusions change when  $r$  is also allowed to vary. The preferred approach to this problem would be to apply the same MCMC analysis on data sets generated from a range of fiducial  $r$ , in addition to  $n_T$ . This method, however, is time consuming and more efficient approaches exist. The previous results from the MCMC analysis show that the posterior distributions of  $r(k_*)$  and  $n_T$  are nearly Gaussian and not too strongly correlated, and so a Fisher matrix analysis should provide reliable constraints (Perotto et al. 2006).

A forecast of parameter constraints can be obtained relatively easily by Taylor expanding the log-likelihood function,  $\ln \mathcal{L}(\boldsymbol{\theta}|\mathbf{d})$ , about the best-fit parameter values,  $\boldsymbol{\theta}$ , and examining the  $2^{nd}$ -order coefficient,

$$F_{ij} = - \left. \frac{\partial^2 \ln \mathcal{L}}{\partial \theta_i \partial \theta_j} \right|_{\boldsymbol{\theta} = \boldsymbol{\theta}}. \quad (21)$$

The Fisher information matrix,  $F_{ij}$ , encodes parameter correlations and measures the steepness of the likelihood function in the direction of each parameter  $\theta_i$ . The minimum precision with which parameter  $\theta_i$  can be measured is set by the Cramer-Rao bound (Tegmark 1997),



$$\sigma_{\theta_i} \geq \sqrt{(F^{-1})_{ii}}. \quad (22)$$

We again consider only the parameters  $r$  and  $n_T$ , and only include B-mode data in the likelihood function (Bond et al. 2000),

$$\begin{aligned} -2 \ln \mathcal{L} = & \sum_{\ell} (2\ell + 1) f_{\text{sky}} \left\{ \ln \left( \frac{C_{\ell}^{BB} + N_{\ell}^{BB}}{\hat{C}_{\ell}^{BB}} \right) \right. \\ & \left. + \frac{\hat{C}_{\ell}^{BB}}{C_{\ell}^{BB} + N_{\ell}^{BB}} - 1 \right\}, \end{aligned} \quad (23)$$

where  $\hat{C}_{\ell}^{BB}$  and  $N_{\ell}^{BB}$  are defined in Eqs. (16) and (20), respectively, and  $C_{\ell}^{BB}$  is the theoretical spectrum. Using Eq. (23) in Eq. (21) gives

$$F_{ij} = \frac{1}{2} \sum_{\ell} (2\ell + 1) f_{\text{sky}} \frac{\partial C_{\ell}^{BB}}{\partial \theta_i} (C_{\ell}^{BB} + N_{\ell}^{BB})^{-2} \frac{\partial C_{\ell}^{BB}}{\partial \theta_j}. \quad (24)$$

We now extend our MCMC analysis of CMBPol and the ideal satellite experiment to examine how these projections vary with fiducial  $r$  (Planck and the ground-based experiments fail to provide strong evidence for  $n_T \neq 0$  consistent with nucleosynthesis constraints even in the optimistic case.) We compute the Fisher matrix Eq. (24) for each experiment on a  $200 \times 200$  grid in the  $(n_T, \log r)$  plane with  $r \in [10^{-6}, 0.4]$  and  $n_T \in [-0.5, 0.5]$ . Having obtained  $\sigma_r$  and  $\sigma_{n_T}$  from Eq. (22), we obtain the Bayes factor via Eq. (4) under the assumption that the marginalized posterior distributions of  $r$  and  $n_T$  are Gaussian. We present results for CMBPol and the ideal satellite experiment in Figure 4. The CMBPol thresholds for strong and decisive evidence are indicated in violet and blue, respectively, and the same thresholds for the ideal experiment are given in orange and red, respectively. For power law spectra, CMBPol will find strong evidence for  $\mathcal{H}_1$  if  $r \geq 0.06$ , and decisive evidence if  $r \geq 0.1$  (in this case confirming the optimistic results of the MCMC analysis, Figure 3.) The ideal experiment has a much better chance of detecting  $n_T \neq 0$ :  $r \geq 10^{-3}$  and  $r \geq 10^{-4}$  for decisive and strong evidence, respectively. The ideal satellite will also find strong evidence in favor of the null hypothesis,  $\mathcal{H}_0$ , for  $r > 2.5 \times 10^{-3}$  and  $n_T$  within the orange dotted contour in Figure 4.

## 5 DISCUSSION

We have obtained projections for the detectability of  $n_T \neq 0$  with current and future satellite and ground-based CMB experiments. Current and proposed missions will struggle to detect a tensor tilt with statistical significance; however, an ideal satellite experiment will perform well. This indicates that discriminating between theories of early Universe structure formation with primordial B-modes is in principle possible using space-based platforms. We now examine the implications of our results for distinguishing between several competing theories for an optimistic detection of  $r = 0.1$ . The following results are summarized in Table 2.

*Inflation:* General inflation predicts a tensor amplitude  $P_h \propto H^2$  at lowest order in slow roll. The dominant energy condition demands that  $\dot{H} < 0$  in a Friedmann Universe, leading to a red tilted tensor spectrum,  $n_T < 0$ . The detection thresholds for the different experiments are presented in Table 1: while large tilts are needed for Planck

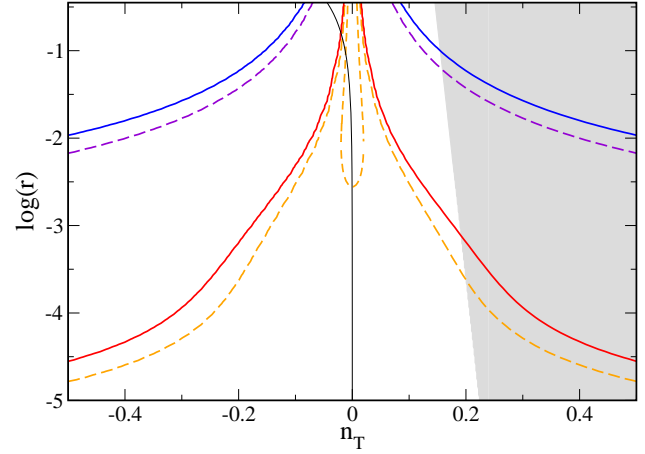


**Figure 4.** Bayes factor as a function of  $r$  and  $n_T$  for CMBPol and the ideal CMB experiment. For CMBPol, thresholds for strong ( $\ln B_{01} = -2.5$ ) and decisive ( $\ln B_{01} = -5$ ) evidence in favor of  $\mathcal{H}_1$  are indicated by the top two contours: violet dashed and blue solid curves, respectively. For the ideal mission, these same thresholds are given by the lower two contours: orange dashed and red solid curves, respectively, and the central closed orange dashed contour indicates the threshold for strong evidence ( $\ln B_{01} = 2.5$ ) favoring the null hypothesis,  $\mathcal{H}_0$ . The interpretation is that inside this contour  $n_T = 0$  is strongly favored over  $n_T \neq 0$ . The gray region is excluded by nucleosynthesis constraints, and the vertically-oriented solid black line gives the prediction of single field slow roll inflation.

and ground-based experiments to make a decisive detection in the most optimistic case, these missions are nonetheless capable of providing evidence in support of inflation. Future missions will improve on these capabilities, but will still require relatively large tilts in the most pessimistic outcome of small  $r$ . Single field inflation predicts a consistency relation,  $r = -8n_T$ , shown as a dashed curve in Figures 4 and 5. Our results indicate that current probes and proposed missions like CMBPol will fail to provide strong evidence in support of single field inflation. If single field inflation is the true source of the B-mode, an ideal experiment will provide decisive supporting evidence if  $n_T < -0.02$ , corresponding to  $r > 0.15$  (c.f. Figure 4).

*String Gases:* During the quasi-static Hagedorn phase of string gas cosmology, the Hubble radius shrinks so that fluctuation modes come to exist on cosmological scales (Nayeri et al. 2006). The anisotropic pressure of the matter fluctuations generates large scale tensor perturbations; this pressure is smaller deep in the Hagedorn phase than it is during the subsequent radiation dominated expansion (Brandenberger et al. 2007). The larger scale tensor modes, which exit the horizon earlier, will therefore have smaller amplitudes than those that exit later, and the resulting tensor spectrum is a power law with a blue tilt. Because it is a power law,  $n_T$  is bound by nucleosynthesis constraints, giving a small window within which  $n_T$  is large enough to be detected, but smaller than the nucleosynthesis cutoff. CMBPol and the ideal satellite will provide strong observational support if  $0.12 < n_T < 0.15$  and  $0.025 < n_T < 0.15$ , respectively.

*Loop Quantum Cosmology:* Motivated by loop quantum gravity, loop quantum cosmology (LQC) is characterized by

**Table 2.** Conditions under which the different experiments will be able to provide strong supporting evidence for different models of early Universe structure formation: single field inflation (SFI), string gases (SG), loop quantum cosmology (LQC), and a nonsingular matter bounce (MB). For LQC, we assume that  $n_T = 2$ , large enough to be decisively detected by all experiments. For the other experiments, supporting evidence is obtained for the fiducial values of  $n_T$  given. These results are for  $r = 0.1$  for all models except SFI, for which strong supporting evidence can only be found for  $r > 0.15$ . See the text for details.

Experiment	SFI	SG	LQC	MB
Planck	No	No	Yes	No
+PolarBear	No	No	Yes	No
+QUIET (II)	No	No	Yes	No
CMBPol	No	$0.12 < n_T < 0.15$	Yes	No
Ideal	$n_T < -0.02$	$0.025 < n_T < 0.15$	Yes	Yes

a quantum bounce joining a prior contracting phase to the expanding phase of big bang cosmology. It was discovered early that inverse volume corrections lead to a period of superinflation ( $w < -1$ ) in the early Universe (Bojowald 2002), generating a power law spectrum of tensor modes with an unacceptably blue tilt (Calcagni & Hossain 2009). More recent analyses have studied the full evolution of the perturbations from their generation during the contracting phase, across the bounce, and through a period of slow roll inflation driven by a massive scalar field (Mielczarek 2010; Mielczarek et al. 2010). Due to the shrinking Hubble radius, modes initiated during the contraction are strongly blue,  $P_h \sim k^2$ . After the bounce, those modes that are outside the horizon are frozen and the blue spectrum is retained on these scales; modes within the horizon after the bounce evolve during the subsequent period of inflation leading to a nearly flat tensor spectrum on smaller scales. The resulting spectrum is effectively a power law with a steep blue spectrum,  $n_T \approx 2$ , on CMB scales, but the non-power law nature of the spectrum allows it to evade the nucleosynthesis constraints. This tensor tilt is large enough to be decisively detected by all the experiments considered in this analysis.

*Matter Bounce:* String cosmology can also accommodate a bouncing Universe. The early implementations, Pre-Big Bang cosmology and the ekpyrotic scenario, included a singular bounce connecting the contracting and expanding phases. Due to the dynamics of the contracting phase, the resulting tensor perturbations in the expanding phase are unacceptably blue in both models, with the requirement that the tensor spectrum be suppressed. Initially introduced as a toy model exhibiting a nonsingular transition, a generic bounce in which the Universe passes from matter to radiation domination prior to the bounce is capable of producing a scale invariant tensor spectrum (Finelli & Brandenberger 2008). Perturbations generated during a collapsing dust dominated Friedmann Universe are identical to those generated during de Sitter expansion (Wands 1999), since the amplitudes of all modes – both sub- and super-horizon – grow at the same rate during dust dominated contraction. This model is our null hypothesis,  $\mathcal{H}_0$ , and it is phenomenologically distinct from all of the other models. If  $n_T = 0$ , an ideal satellite will provide strong evidence for it.

Although we have not considered them in this work, it is expected that future space-based laser interferometers like Big Bang Observer and Japan’s Deci-hertz Interferometer Gravitational Wave Observatory (DECIGO) will measure  $n_T$  at least as precisely as an ideal CMB satellite (Seto 2006; Kudoh et al. 2006; Zhao & Baskaran 2009) and should

perform well under Bayesian model selection; we leave this analysis for future work. In the meantime, we can conclude that the awesome prospect of using the primordial B-mode as a window into the origin of structure formation will be within the grasp of next-generation space probes.

## REFERENCES

- Baumann D., *et al.* [CMBPol Study Team Collaboration], 2009, AIP Conf. Proc. **1141**, 3  
Baumann D., Zaldarriaga M., 2009, JCAP **0906**, 013  
Beltran M., Garcia-Bellido J., Lesgourgues J., Liddle A., Slosar A., 2005, Phys. Rev. D **71**, 063532  
Bojowald M., 2002, Phys. Rev. Lett. **89**, 261301  
Bond J. R., Jaffe A. H., Knox L. E., 2000, Astrophys. J. **533**, 19  
Brandenberger R., 2011, [arXiv:1104.3581 [astro-ph.CO]].  
Brandenberger R. H., Nayeri A., Patil S. P., Vafa C., 2007 Phys. Rev. Lett. **98**, 231302  
Calcagni G., Hossain G. M., 2009, Adv. Sci. Lett. **2**, 184  
Dickey J. M., 1971, Ann. Math. Stat., **42**, 204  
Finelli F., Brandenberger R., 2002, Phys. Rev. D **65**, 103522  
Fraisie A. A., *et al.*, 2008, *CMBPol Mission Concept Study: Foreground Science Knowledge and Prospects*, [arXiv:0811.3920 [astro-ph]].  
Garcia-Bellido J., Durrer R., Fenu E., Figueroa D. G., Kunz M., 2011, Phys. Lett. B **695**, 26  
Hirata C. M., Seljak U., 2003, Phys. Rev. D **68**, 083002  
Hu W., Okamoto T., 2002, Astrophys. J. **574**, 566  
Jaynes E., 2003, *Probability Theory: The Logic of Science*. Cambridge University Press  
Jeffreys H., 1961, *Theory of Probability*, 3rd ed, Oxford University Press  
Jones-Smith K., Krauss L. M., Mathur H., 2008, Phys. Rev. Lett. **100**, 131302  
Kamionkowski M., Kosowsky A., Stebbins A., 1997, Phys. Rev. D **55**, 7368  
Kamionkowski M., Kosowsky A., Stebbins A., 1997, Phys. Rev. Lett. **78**, 2058  
Knox L., 1995, Phys. Rev. D **52**, 4307  
Komatsu E., *et al.* [WMAP Collaboration], 2011, Astrophys. J. Suppl. **192**, 18  
Kudoh H., Taruya A., Hiramatsu T., Himemoto Y., 2006, Phys. Rev. D **73**, 064006  
Lewis A., Bridle S., 2002, Phys. Rev. D **66**, 103511  
Lewis A., Challinor A., Lasenby A., 2000, Astrophys. J. **538**, 473

- Liddle A. R., Mukherjee P., Parkinson D., 2006, [arXiv:astro-ph/0608184].
- Lindley D., 1957, *Biometrika*, **44**, 187
- Ma Y. Z., Zhao W., Brown M. L., 2010, *JCAP* **1010**, 007
- MacKay D., 2003, *Information Theory, Inference, and Learning Algorithms*. Cambridge University Press
- Mukherjee P., Parkinson D., 2008, *Int. J. Mod. Phys. A* **23** 787
- Mielczarek J., 2010, *Phys. Rev. D* **81**, 063503
- Mielczarek J., Cailleteau T., Grain J., Barrau A., 2010, *Phys. Rev. D* **81**, 104049
- Mukherjee P., Parkinson D., Liddle A. R., 2006, *Astrophys. J.* **638**, L51
- Nayeri A., Brandenberger R., Vafa C., 2006, *Phys. Rev. Lett.* **97**, 021302
- Pahud C., Liddle A. R., Mukherjee P., Parkinson D., 2006, *Phys. Rev. D* **73**, 123524
- Perotto L., Lesgourgues J., Hannestad S., Tu H., Wong Y. Y., 2006, *JCAP* **0610**, 013
- Planck Collaboration, 2006, *The Scientific Programme of Planck* [arXiv:astro-ph/0604069].
- Pogosian L., Wyman M., 2008, *Phys. Rev. D* **77**, 083509
- O’Ruanaidh J. J. K., Fitzgerald W. J., 1996, *Numerical Bayesian Methods Applied to Signal Processing*. Springer-Verlag, New York
- Piao S. Y., Zhang Y. Z., 2004, *Phys. Rev. D* **70**, 063513
- Samtleben D. et al. [QUIET Collaboration], 2007, *Nuovo Cim. B* **122**, 1353
- Seljak U., Hirata C. M., 2004, *Phys. Rev. D* **69**, 043005
- Seljak U., Slosar A., 2006, *Phys. Rev. D* **74**, 063523
- Seljak U., Zaldarriaga M., 1997 *Phys. Rev. Lett.* **78**, 2054
- Seto N., 2006, *Phys. Rev. D* **73**, 063001
- Shafer G., 1982, *J. Am. Stat. Assoc.* Vol. 77, No. 378
- Skilling J., 2004, unpublished, available from <http://www.inference.phy.cam.ac.uk/bayesys/>.
- Stewart A., Brandenberger R., 2008, *JCAP* **0808**, 012
- Tegmark M., Taylor A., Heavens A., 1997, *Astrophys. J.* **480**, 22
- Trotta R., 2005, *Mon. Not. Roy. Astron. Soc.* **378**, 72
- Trotta R., 2008, *Contemp. Phys.* **49**, 71
- Urrestilla J., Mukherjee P., Liddle A. R., Bevis N., Hindmarsh M., Kunz M., 2008, *Phys. Rev. D* **77**, 123005
- Vardanyan M., Trotta R., Silk J., 2009, *Mon. Not. Roy. Astron. Soc.* **397**, 431
- Verde L., Peiris H., Jimenez R., 2006 *JCAP* **0601**, 019
- Wands D., 1999, *Phys. Rev. D* **60**, 023507
- Zaldarriaga M., Seljak U., 1998 *Phys. Rev. D* **58**, 023003
- Zhao W., Baskaran D., 2009 *Phys. Rev. D* **79**, 083003
- Zhao W., Zhang W., 2009 *Phys. Lett. B* **677**, 16